CCS Chemistry

COMMUNICATION

Received: June 2, 2020 | Accepted: July 28, 2020

Live-Cell Imaging of NADPH Production from Specific Pathways

Senlian Hong[1,2,3†‡], Tao Chen[4,5,6†‡], Ling Liu[7,8], Chen Cao[4,5,6], Fengxiang Lv[9], Joshua D. Rabinowitz[7,8], Yanyi Huang[1,2,3,4,5,6,10*] & Xing Chen[1,2,3,11,12*]

[1]College of Chemistry and Molecular Engineering, Peking University, Beijing 100871, [2]Peking-Tsinghua Center for Life Sciences, Peking University, Beijing 100871, [3]Beijing National Laboratory for Molecular Sciences, Peking University, Beijing 100871, [4]College of Engineering, Peking University, Beijing 100871, [5]Biomedical Pioneering Innovation Center, Peking University, Beijing 100871, [6]Beijing Advanced Innovation Center for Genomics, Peking University, Beijing 100871, [7]Lewis-Sigler Institute for Integrative Genomics, Princeton University, Princeton, NJ 08544, [8]Department of Chemistry, Princeton University, Princeton, NJ 08544, [9]Institute of Molecular Medicine, Peking University, Beijing 100871, [10]Shenzhen Bey Laboratory, Institute for Cell Analysis, Peking University, Beijing 100871, [11]Synthetic and Functional Biomolecule Center, Peking University, Beijing 100871, [12]Key Laboratory of Bioorganic Chemistry and Molecular Engineering of Ministry of Education, Peking University, Beijing 100871

**Corresponding authors: yanyi@pku.edu.cn; xingchen@pku.edu.cn;* [†]S. Hong and T. Chen contributed equally to this work.
[‡]Present address: S. Hong is currently with Department of Molecular Medicine, The Scripps Research Institute, La Jolla, CA 92037 and T. Chen is currently with Huffington Center on Aging, Baylor College of Medicine, Houston, TX 77030.

Cite this: *CCS Chem.* **2020**, *2*, 1642–1648

As anconversion of essential cofactor for lipid biosynthesis and antioxidant defense, reduced nicotinamide adenine dinucleotide phosphate (NADPH) is produced via various pathways, including the oxidative pentose phosphate pathway (oxPPP) and the malic enzyme 1 (ME1)-catalyzed conversion of malate to pyruvate. Live-cell detection of NADPH production routes remains challenging. Here, we report tracing hydrides into lipid droplets (THILD), a chemical imaging strategy for the detection of pathway-specific NADPH generation in live cells. This strategy exploits deuterium (^{2}H)-labeled glucose ([^{2}H]Glc) tracers that transfer deuterides to NADPH via specific pathways. The NADP^{2}H, in turn, transfers deuterides to lipids, resulting in accumulation of C–^{2}H bonds in lipid droplets, which can be visualized by bioorthogonal stimulated Raman scattering (SRS) microscopy. We used this concept to demonstrate the imaging of oxPPP-produced NADPH using the oxPPP-specific tracer, [3-^{2}H]Glc. Furthermore, the "switch on" of NADPH production by ME1 in differentiating adipocytes was imaged by [4-^{2}H]Glc. Finally, comparison of [3-2H]Glc and [4-2H]Glc THILD imaging of adipocytes showed that hypoxia induces suppression of ME1-mediated NADPH production and oxPPP-produced NADPH becomes the main source.

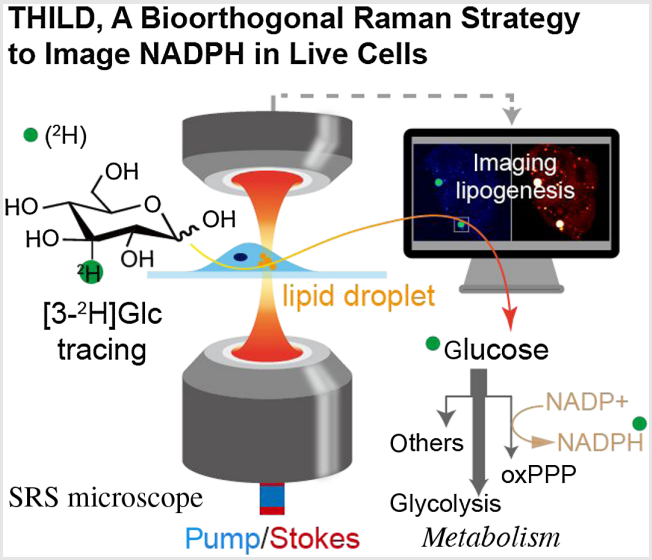

Keywords: NADPH, metabolic reprogramming, bioorthogonal Raman imaging, deuterium tracing, SRS microscopy, pathway specificity

DOI: 10.31635/ccschem.020.202000346
CCS Chem. **2020**, *2*, 1642–1648

Introduction

As a carrier for high-energy electrons, reduced nicotinamide adenine dinucleotide phosphate (NADPH) is an essential cofactor for supplying the reducing power for lipid biosynthesis and maintaining redox homeostasis in living cells. NADPH is produced in various pathways, including the oxidative pentose phosphate pathway (oxPPP), folate metabolism, and malic enzyme 1 (ME1)-mediated conversion of malate to pyruvate.[1,2] The contribution of different NADPH-producing pathways or enzymes for maintaining cellular physiology is cell-type dependent and varies in response to the redox status of cells. Aberrant NADPH metabolism has been implicated in various health conditions, such as cancer and aging.[3–5] Therefore, detection and quantification of cellular NADPH pools are of great importance for understanding a variety of essential biochemical and pathological processes.

Currently, fluorescence microscopy and mass spectrometry (MS) are two complementary approaches for NADPH analysis, each of which has its own strengths and limitations. NADPH can be visualized directly in live cells by using fluorescence lifetime imaging microscopy (FLIM), which exploits the characteristic fluorescence lifetime of the nicotinamide ring in its enzyme-bound state.[6] Moreover, genetically encoded and semisynthetic fluorescent sensors have recently been developed for imaging and quantifying NADPH concentrations in living cells.[7,8] Although fluorescent imaging allows analysis of the overall NADPH at the live single-cell level, it is unable to differentiate NADPH made by different production pathways. Alternatively, NADPH can be labeled isotopically in a pathway-specific manner by using stable isotope tracers and MS detection.[9] Specifically, deuterium (^{2}H)-labeled glucose ([^{2}H]Glc) tracers have been used to report the transfer of the deuterium-labeled hydride (i.e., deuteride) to NADPH, resulting in deuterium-labeled NADPH (i.e., NADP^{2}H). For example, [3-^{2}H]Glc can serve as a tracer for detecting NADPH produced by the oxPPP. The deuteride at carbon-3 (C-3) is transferred to NADP^{2}H by the oxPPP enzyme 6-phosphogluconate dehydrogenase (6PGD), and the NADP^{2}H generated is detected and quantified by liquid chromatography-mass spectrometry (LC-MS).[10,11] Similarly, [4-^{2}H]Glc specifically reports on NADP^{2}H produced by the malic enzyme.[12] Nonetheless, despite providing pathway specificity, the MS-based measurements have to be performed in cell extracts and use a large quantity of cells.

Herein, we report the development of tracing hydrides into lipid droplets (THILD), a chemical imaging strategy for pathway-specific visualization of NADPH in live cells (Figures 1a and 1b). THILD employs stimulated Raman scattering (SRS) microscopy[13] to visualize carbon–deuterium (C–^{2}H) bonds in lipid droplets (LDs), for which the deuteride is transferred from NADP^{2}H during fatty acid synthesis. By using pathway-specific [^{2}H]Glc tracers, bioorthogonal Raman imaging of LDs could be employed to report on the production of NADPH from respective pathways. Unlike conventional NADPH analysis methods based on fluorescence microscopy and MS, THILD combines the strengths of both techniques to offer an integrative solution.

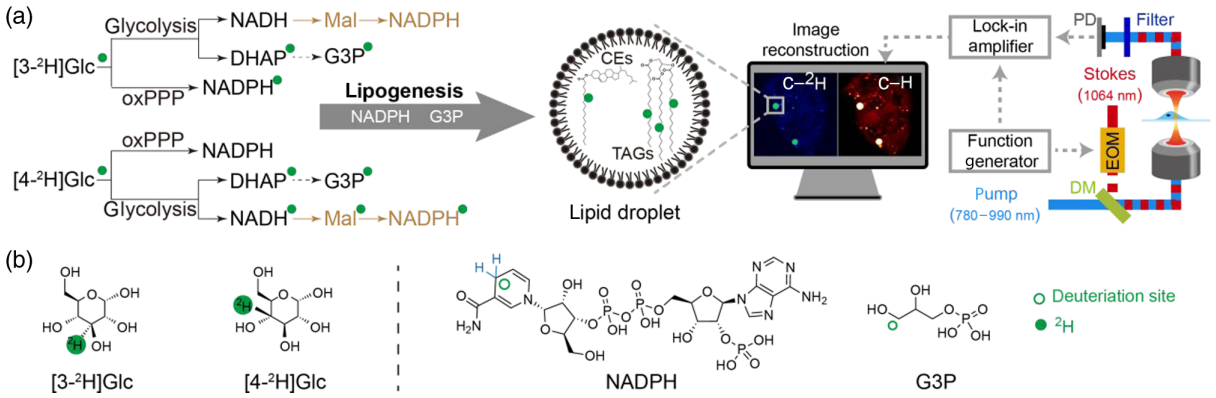

Figure 1 | *THILD enables pathway-specific imaging of NADPH production in live cells. (a) The flow of the deuteride of [3-^{2}H]Glc and [4-^{2}H]Glc to metabolites through glycolysis, oxPPP, and/or ME1. The deuterium-labeled NADPH and G3P are used for lipogenesis, which results in the accumulation of C–^{2}H in LDs. Bioorthogonal SRS microscopy at 2145 cm^{-1} for C–^{2}H in LDs, which is termed THILD, hence exhibits NADPH production in living cells. The dash lines indicate an insignificant contribution to the THILD signal. Note that ME1-mediated production of NADPH is only active in adipocytes but not HepG2 cells. (b) Chemical structures of [3-^{2}H]Glc, [4-^{2}H]Glc, NADPH, and G3P. NADPH, reduced nicotinamide adenine dinucleotide phosphate; oxPPP, oxidative pentose phosphate pathway; ME1, malic enzyme 1; G3P, glyceraldehyde 3-phosphate, LDs, lipid droplets; SRS, stimulated Raman scattering; THILD, tracing hydrides into lipid droplets.*

DOI: 10.31635/ccschem.020.202000346
CCS Chem. **2020**, *2*, 1642–1648

Results and Discussion

Specific chemical bonds such as C–^{2}H possess Raman scattering within the Raman-silent region of a cell between ~1900 and ~2700 cm^{-1}. Because endogenous biomolecules do not produce any Raman signal in this silent region, these chemical bonds can be exploited as bioorthogonal Raman reporters to tag biomolecules for live-cell imaging.[14,15] Although, in principle, NADP^{2}H could be directly imaged by Raman microscopy, it remains practically challenging due to the intrinsically weak signal. Even with SRS, which dramatically improves the detection sensitivity of spontaneous Raman spectroscopy,[13] the cellular concentration of NADPH (~100 μM)[16] is below the detection limit. To solve this problem, THILD exploits fat synthesis, the most NADPH-demanding pathway that transfers and accumulates deuteride of NADP^{2}H to the C–^{2}H bonds of lipids in LDs. Owing to the extremely high lipid concentration in LDs,[17] the C–^{2}H signal is highly enriched in LDs and exceeds that of other deuterium-labeled molecules in cells; thereby, enabling specific SRS imaging of LDs with high contrast.

We first sought to demonstrate THILD by imaging oxPPP-produced NADPH using [3-^{2}H]Glc as the tracer. Lipogenesis is NADPH dependent and therefore accumulates C–^{2}H in newly synthesized fatty acids and cholesterol,[10,11] which are major components of LDs.[17] HepG2 cells, a human hepatic cell line with active lipogenesis, were incubated with [3-^{2}H]Glc for 2 days. The spontaneous Raman spectra of [3-^{2}H]Glc-treated cells exhibited a C–^{2}H peak at ~2145 cm^{-1}, which fell into the silent region, and therefore, was not interfered by intrinsic Raman signals of cellular molecules (Figure 2a and Supporting Information Figure S1). SRS spectra showed the C–^{2}H peak at the same frequency, confirming the specificity of SRS microscopy at 2145 cm^{-1} for C–^{2}H in live cells (Figure 2a and Supporting Information Figure S2). The [3-^{2}H]Glc-treated cells were stained with the BODIPY dye to visualize LDs,[18] which were then imaged by SRS microscopy and confocal fluorescence microscopy (Figure 2b). Spherical droplets delimited by the SRS signal of C–^{2}H colocalized well with the C–H SRS signal at 2845 cm^{-1}, which has been widely used to visualize LDs.[19–21] Collectively, these results demonstrated that the catabolism of [3-^{2}H]Glc resulted in the accumulation of C–^{2}H in LDs, which was then visualized directly by SRS microscopy at 2145 cm^{-1}.

Further, we validated that THILD imaging using [3-^{2}H]Glc could specifically manifest the NADPH production via the oxPPP pathway. There are several pathways through which [^{2}H]Glc could transfer deuterides to metabolites used for lipogenesis: (1) through glycolysis, the ^{2}H could be transferred to glycerol 3-phosphate (G3P), (2) the glycolysis-produced pyruvate could enter the mitochondria and transfers ^{2}H to acetyl-coenzyme A (AcCoA), which could be transported to the cytoplasm via the citrate shuttle, and (3) through the oxPPP pathway, ^{2}H could be transferred to NADPH. With NADPH and AcCoA used in the fatty acid synthesis and G3P in the triglyceride synthesis during lipogenesis, the three metabolites link Glc catabolism with packaging triglycerides within LDs (Supporting Information Figure S3a). Notably, for [3-^{2}H]Glc, the ^{2}H at C-3 is transferred to NADPH and G3P, but not AcCoA (Figure 2c and Supporting Information Figure S3b). To quantify the contribution of the THILD signal in LDs from individual metabolites, we employed the LC-MS method[10,11] to track deuterium transfer in the [3-^{2}H]Glc-treated cell lysates (Figure 2c). Approximately 25% NADPH was labeled with deuterium, while ~18% G3P was labeled (Figure 2d). As expected, AcCoA was not labeled. We also confirmed that ^{2}H was transferred effectively into fatty acids, including myristate, palmitate, and stearate (Figure 2e). These results were in agreement with the previous data,[10,11] with slight variations on labeling ratios, attributable to differences in cell lines and incubation times. Biosynthesis of one molecule of glycerol tripalmitate (as an example), it consumes 52 molecules of NADPH and one molecule of G3P, resulting in their contributions of ^{2}H in glycerol tripalmitate to be 98.7% and 1.3%, respectively (Supporting Information Figure S3c). With the C–^{2}H SRS signals in LDs mostly from NADPH, [3-^{2}H]Glc THILD can be used to probe NADPH production by the oxPPP pathway in live cells.

To normalize the variation of lipid concentration within different LDs, we defined THILD intensity as the proportion of C–^{2}H bonds in the total carbon–hydrogen bonds, including C–^{2}H and C–H bonds, calculated using the formula [C–^{2}H]/([C–^{2}H] + [C–H]) (see Supporting Information Section "Experimental Procedures"). Then THILD distribution was obtained in each cell (Figure 2b, bottom right panel). The NADPH production via oxPPP in HepG2 cells was visualized readily by THILD using [3-^{2}H]Glc in 1 day, and the THILD signal accumulated to saturation by 2 days (Figure 2f). When the [3-^{2}H]Glc-treated cells were chased in normal media containing Glc, the THILD signal was mostly lost within 1 day (Figure 2g). Additionally, the THILD signal diminished via inhibition of the fatty acid synthase enzyme (Figure 2h). These results demonstrated that the turnover of lipogenesis from Glc is at the time scale of several days, which is well suited for THILD.

Next, we expanded the tracer repertoire to various [^{2}H]Glc molecules for THILD imaging in HepG2 cells (Figure 3a). Based on the biochemical reactions in the conversion of glucose to lipids, different [^{2}H]Glc tracers have distinct capabilities of transferring deuterides to NADPH, AcCoA, and G3P (Supporting Information Figure S3b). An LC-MS analysis confirmed the ^{2}H transfer profiles of [^{2}H]Glc and revealed the labeling ratios of three metabolites (Figure 3b) and fatty acids (Supporting Information Figure S4). [1-^{2}H]Glc produced

DOI: 10.31635/ccschem.020.202000346
CCS Chem. **2020**, *2*, 1642–1648

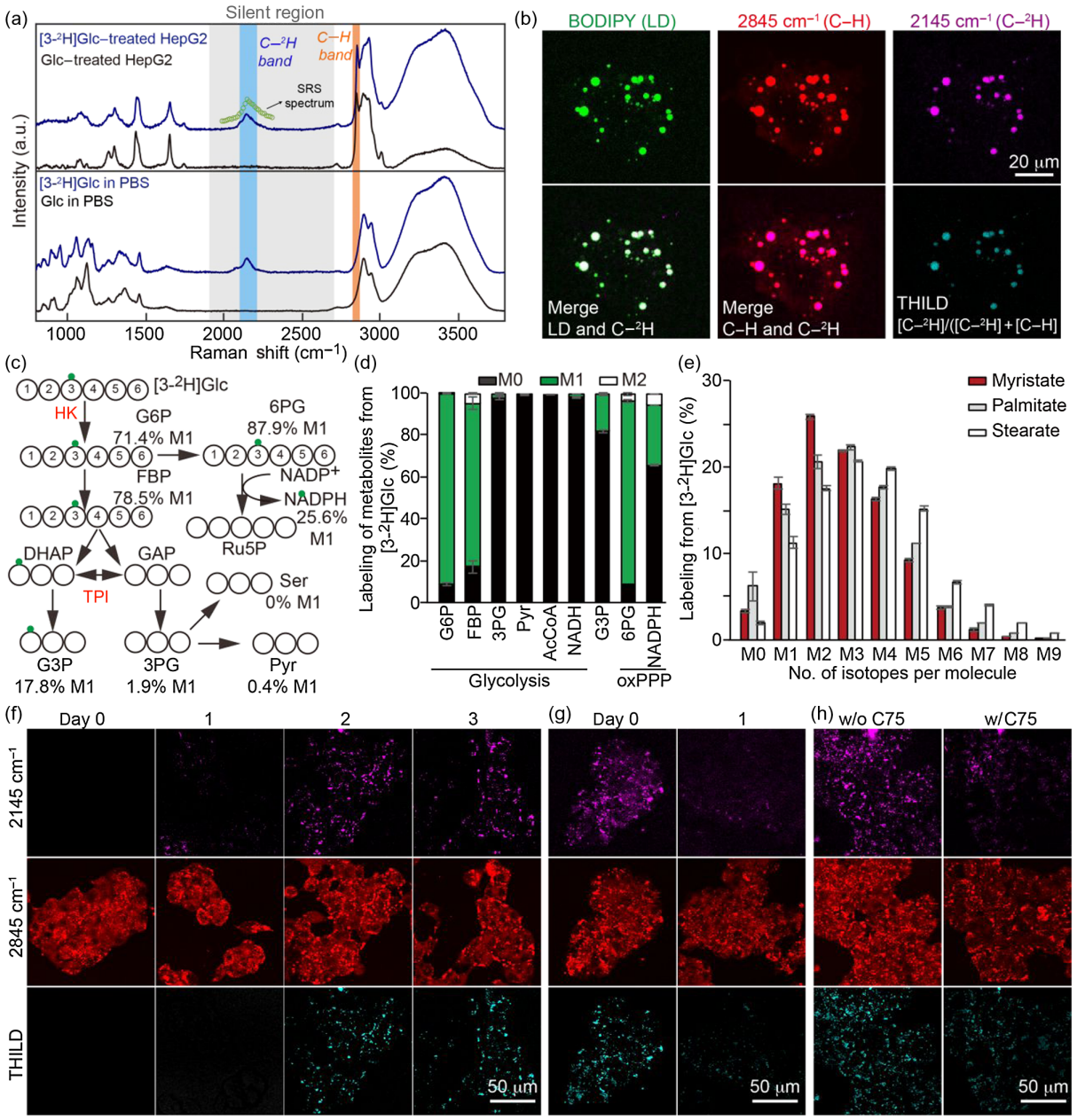

Figure 2 | *THILD imaging of oxPPP-produced NADPH by [3-²H]Glc in live cells. (a) Spontaneous Raman spectra of HepG2 cells cultured in [3-²H]Glc or Glc, and phosphate-buffered saline (PBS) solutions of [3-²H]Glc and Glc. The green curve shows the SRS spectrum mapped from the [3-²H]Glc-treated cells. (b) SRS, fluorescence, and THILD images of HepG2 cells treated with 25 mM [3-²H]Glc for 2 days, followed by staining with BODIPY. Scale bar, 20 μm. (c) Schematic showing the flow of the [3-²H]Glc hydride through oxPPP and glycolysis. Open circles represent carbon, and green dots represent deuterium. The numbers below the metabolites indicate deuterium labeling ratios. (d) Labeling of metabolites in HepG2 cells treated with [3-²H]Glc, followed by analysis by LC-MS. NADPH was measured at 20 min and the rest at 2 h. (e) Labeling of fatty acids in HePG2 cells treated with [3-²H]Glc for 2 days. (f–h) THILD and SRS images of HepG2 cells treated with 25 mM [3-²H]Glc for varied durations of time (f), incubated with 25 mM [3-²H]Glc for 2 days, followed by chasing with Glc for 1 day, and incubated with 25 mM [3-²H]Glc for 2 days, in the presence and absence of a fatty acid synthase inhibitor C75 (h). For SRS imaging, the channels of C–²H at 2145 cm⁻¹ and C–H at 2845 cm⁻¹ are shown. In (d and e), error bars represent mean ± SD. The results are from three independent experiments. In (b, f, g, and h), scale bars, 50 μm. THILD, tracing hydrides into lipid droplets; oxPPP, oxidative pentose phosphate pathway; NADPH, reduced nicotinamide adenine dinucleotide phosphate; Glc, glucose; SRS, stimulated Raman scattering; LC-MS, liquid chromatography mass spectrometry.*

DOI: 10.31635/ccschem.020.202000346
CCS Chem. **2020**, *2*, 1642–1648

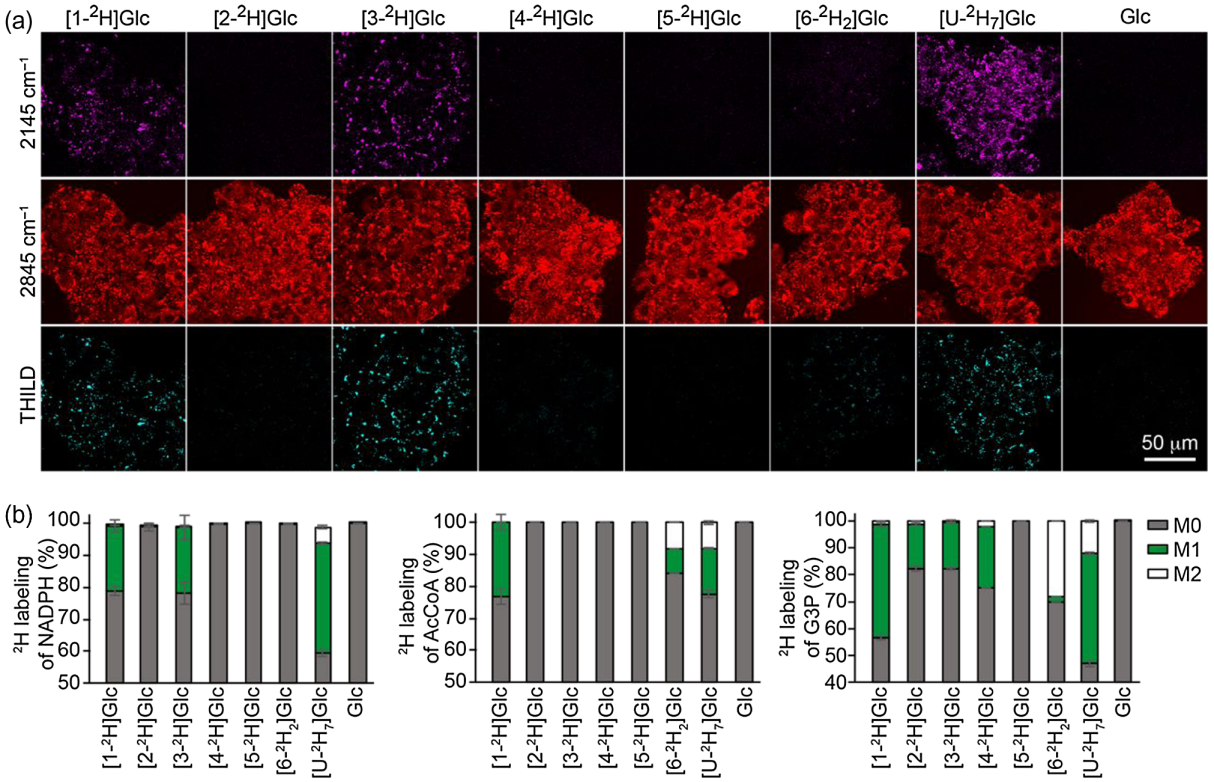

Figure 3 | *THILD imaging using various [²H]Glc tracers. (a) THILD and SRS images of HepG2 cells incubated with 25 mM [1-²H]Glc, [2-²H]Glc, [3-²H]Glc, [4-²H]Glc, [5-²H]Glc, [6,6-²H₂]Glc, [U-⁷H]Glc, or Glc for 2 days. For SRS imaging, the channels of C–²H at 2145 cm⁻¹ and C–H at 2845 cm⁻¹ are shown. Scale bar, 50 μm. (b) ²H labeling of NADPH, AcCoA, and G3P from various [²H]Glc tracers at 25 mM in HepG2 cells. NADPH was measured from cells treated with tracers for 20 min, and AcCoA and G3P were measured at 2 h by LC-MS. M0, M1, and M2 are isotopomers with no, one, and two ²H atoms, respectively. Error bars represent mean ± SD. The results are from three independent experiments. THILD, tracing hydrides into lipid droplets; SRS, stimulated Raman scattering; NADPH, reduced nicotinamide adenine dinucleotide phosphate; AcCoA, acetyl-coenzyme A; G3P, glyceraldehyde 3-phosphate; LC-MS, liquid chromatography mass spectrometry.*

THILD signals from all three metabolites. [2-²H]Glc and [4-²H]Glc only labeled G3P, resulting in a weak THILD signal. [5-²H]Glc did not result in G3P labeling, as shown by LC-MS, probably due to a signal loss by deuterium exchange with H_2O in the step that converts glyceraldehyde 3-phosphate (GAP) to dihydroxyacetone phosphate (DHAP). [6,6-²H_2]Glc-labeled G3P and AcCoA and detectable THILD signals were observed. [U-²H_7]Glc, with all the C–H bonds substituted with deuterium, exhibited strong THILD signals, and it was well suited for SRS imaging of de novo lipogenesis.[22] Similar results were observed in LNCaP and Raw264.7 cells, demonstrating the generic applicability of THILD in various cell types (Supporting Information Figure S5).

We demonstrated further the versatility of THILD by exploiting the combination of two tracers, [4-²H]Glc and [3-²H]Glc, to visualize NADPH production in adipocytes (Figures 4a and 4b). In adipocytes, ME1 and adenosine 5′-triphosphate (ATP)-citrate lyase are upregulated, which, together with malate dehydrogenase, can generate NADPH from reduced nicotinamide adenine dinucleotide (NADH).[23] ME1 is a major NADPH producer in adipocytes but not preadipocytes, as determined by LC-MS using metabolic tracers, including [4-²H]Glc.[12] We then applied THILD to detect this "switch off" of NADPH production pathways by live-cell imaging. 3T3-L1 preadipocytes were differentiated into adipocytes, and the two types of cells were used for comparison. Since [4-²H]Glc-labeled G3P contributed insignificantly to lipid labeling, compared with NADPH, [4-²H]Glc could serve as a THILD tracer specific for ME1-produced NADPH. As expected, in 3T3-L1 preadipocytes [3-²H]Glc THILD signals corresponding to oxPPP-produced NADPH were detected, but there was no observation of ME1 production of NADPH in the [4-²H]Glc THILD imaging (Supporting Information Figure S6a).

Upon differentiation to adipocytes, strong [4-²H]Glc THILD signals were observed, indicating "switch on" of the ME1-mediated NADPH production (Figure 4a). By comparing the [4-²H]Glc THILD signal with the [3-²H]Glc

DOI: 10.31635/ccschem.020.202000346
CCS Chem. **2020**, *2*, 1642–1648

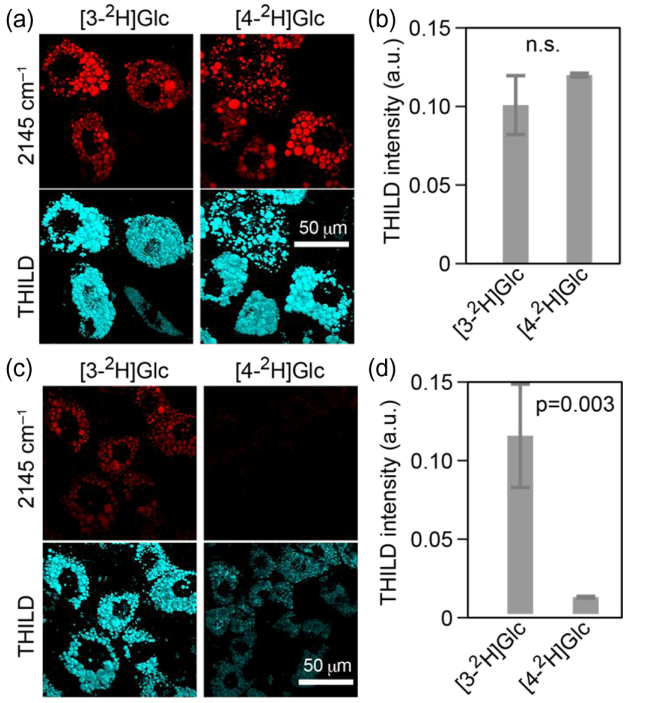

Figure 4 | *THILD imaging of NADPH production in adipocytes. (a and c) THILD and SRS images of differentiating 3T3-L1 adipocytes treated with 25 mM [3-^{2}H]Glc or [4-^{2}H]Glc in conditions of normoxia (a) and hypoxia (c). For SRS imaging, the channel of C–^{2}H at 2145 cm^{-1} is shown. Scale bar, 50 μm. (b and d) Statistical analysis of THILD intensity of cells in conditions of normoxia (b) and hypoxia (d). Error bars represent mean ± SD. Results are from at least 10 cells from three independent experiments. The significance was assessed via unpaired two-tailed Student's* t *test, and* p *value was provided. Note: n.s. represents not significant (*$p \geq 0.05$*). THILD, tracing hydrides into lipid droplets; NADPH, reduced nicotinamide adenine dinucleotide phosphate; SRS, stimulated Raman scattering.*

THILD signal, the relative contributions of ME1 and oxPPP to NADPH production are at an about 1:1 ratio, with oxPPP being a little less (Figure 4b). In hypoxia, ME1 in adipocytes is downregulated, thus, switching the NADPH production toward oxPPP.[12] Accordingly, comparison of THILD [4-^{2}H]Glc and [3-^{2}H]Glc imaging revealed that NADPH production from ME1 was significantly suppressed and oxPPP-produced NADPH became the dominant source in adipocytes in hypoxia (Figures 4c and 4d).

Conclusion

We have developed a chemical imaging strategy, THILD, for monitoring cellular NADPH production routes. THILD combines two features: live-cell detection and pathway specificity. Other current methods provide only one of these features. For example, the MS-based methods cannot be performed in live cells, and fluorescence microscopy-based approaches cannot distinguish NADPH generation from distinct pathways. Favorably, THILD provides a new approach to investigate NADPH-related cellular metabolism pathways in live cells, which is complementary to the current methods. For example, fluorescence microscopy-based methods offer direct visualization of NADPH, which enables monitoring of the dynamic changes of NADPH with better time resolution.

In principle, THILD could be applied to detect other metabolites. For example, [6,6-$^2H_2$]Glc labels AcCoA and G3P (Supporting Information Figure S3b). Because synthesizing a molecule of glycerol tripalmitate uses 24 AcCoA molecules and one G3P molecule (Supporting Information Figure S3c), [6,6-$^2H_2$]Glc likely serves as an AcCoA-specific tracer. Besides, [4-^{2}H]Glc labels cytosolic NADH, which is upstream of NADPH (Figure 4a). Thus, it would be an interesting future direction to investigate these metabolic pathways in live cells using THILD. Of note, SRS currently has a detection limitation on C–^{2}H in the millimolar (mM) range, which limits the detection sensitivity of THILD. With future improvements on the sensitivity of SRS, THILD might be applied to monitor faster dynamics in cellular metabolism.

Supporting Information

Supporting Information is available.

Conflict of Interest

The authors declare no conflict of interests.

Acknowledgments

This project is supported by the National Natural Science Foundation of China (nos. 91753206 and 21521003 to X.C; nos. 21327808 and 21525521 to Y.H.), the National Key R&D Program of China (no. 2018YFA0507600 to X.C. and no. 2018YFA0108100 to Y.H.), the 2018 Beijing Brain Initiation (no. Z181100001518004 to Y.H.), the Beijing Advanced Innovation Center for Genomics (Y.H.), the US National Institutes of Health (no. R01CA163591 to J.D.R.), and the China Postdoctoral Science Foundation (no. 2015M580009 to S.H.).

References

1. Ying, W. NAD+/NADH and NADP+/NADPH in Cellular Functions and Cell Death: Regulation and Biological Consequences. *Antioxid. Redox Signal.* **2008**, *10*, 179–206.

2. Lunt, S. Y.; Vander Heiden, M. G. Aerobic Glycolysis: Meeting the Metabolic Requirements of Cell Proliferation. *Annu. Rev. Cell Dev. Biol.* **2011**, *17*, 441–464.
3. Jeon, S. M.; Chandel, N. S.; Hay, N. AMPK Regulates NADPH Homeostasis to Promote Tumour Cell Survival During Energy Stress. *Nature* **2012**, *485*, 661–665.
4. Patra, K. C.; Hay, N. The Pentose Phosphate Pathway and Cancer. *Trends Biochem. Sci.* **2014**, *39*, 347–354.
5. Nóbrega-Pereira, S.; Fernandez-Marcos, P. J.; Brioche, T.; Gomez-Cabrera, M. C.; Salvador-Pascual, A.; Flores, J. M.; Vina, J.; Serrano, M. G6PD Protects from Oxidative Damage and Improves Healthspan in Mice. *Nat. Commun.* **2016**, *7*, 10894.
6. Blacker, T. S.; Mann, Z. F.; Gale, J. E.; Ziegler, M.; Bain, A. J.; Szabadkai, G.; Duchen, M. R. Separating NADH and NADPH Fluorescence in Live Cells and Tissues Using FLIM. *Nat. Commun.* **2014**, *5*, 3936.
7. Tao, R.; Zhao, Y.; Chu, H.; Wang, A.; Zhu, J.; Chen, X.; Zou, Y.; Shi, M.; Liu, R.; Su, N.; Du, J.; Zhou, H. M.; Zhu, L.; Qian, X.; Liu, H.; Loscalzo, J.; Yang, Y. Genetically Encoded Fluorescent Sensors Reveal Dynamic Regulation of NADPH Metabolism. *Nat. Methods* **2017**, *14*, 720–728.
8. Sallin, O.; Reymond, L.; Gondrand, C.; Raith, F.; Koch, B.; Johnsson, K. Semisynthetic Biosensors for Mapping Cellular Concentrations of Nicotinamide Adenine Dinucleotides. *Elife* **2018**, *7*, 783.
9. Jang, C.; Chen, L.; Rabinowitz, J. D. Metabolomics and Isotope Tracing. *Cell* **2018**, *273*, 822–837.
10. Fan, J.; Ye, J.; Kamphorst, J. J.; Shlomi, T.; Thompson, C. B.; Rabinowitz, J. D. Quantitative Flux Analysis Reveals Folate-Dependent NADPH Production. *Nature* **2014**, *510*, 298–302.
11. Lewis, C. A.; Parker, S. J.; Fiske, B. P.; McCloskey, D.; Gui, D. Y.; Gree, C. R.; Vokes, N. I.; Feist, A. M.; Vander Heiden, M. G.; Metallo, C. M. Tracing Compartmentalized NADPH Metabolism in the Cytosol and Mitochondria of Mammalian Cells. *Mol. Cell* **2014**, *55*, 253–263.
12. Liu, L.; Shah, S.; Fan, J.; Park, J. O.; Wellen, K. E.; Rabinowitz, J. D. Malic Enzyme Tracers Reveal Hypoxia-Induced Switch in Adipocyte NADPH Pathway Usage. *Nat. Chem. Biol.* **2016**, *12*, 345–352.
13. Cheng, J. X.; Xie, X. S. Vibrational Spectroscopic Imaging of Living Systems: An Emerging Platform for Biology and Medicine. *Science* **2015**, *350*, aaa8870.
14. Hong, S.; Lin, L.; Xiao, M.; Chen, X. Live-Cell Bioorthogonal Raman Imaging. *Curr. Opin. Chem. Biol.* **2015**, *24*, 91–96.
15. Shen, Y.; Hu, F.; Min, W. Raman Imaging of Small Biomolecules. *Annu. Rev. Biophys.* **2019**, *48*, 347–369.
16. Lu, W.; Wang, L.; Chen, L.; Hui, S.; Rabinowitz, J. D. Extraction and Quantitation of Nicotinamide Adenine Dinucleotide Redox Cofactors. *Antioxid. Redox Signal.* **2018**, *28*, 167–179.
17. Olzmann, J. A.; Carvalho, P. Dynamics and Functions of Lipid Droplets. *Nat. Rev. Mol. Cell Biol.* **2019**, *20*, 137–155.
18. Listenberger, L. L.; Brown, D. A. Fluorescent Detection of Lipid Droplets and Associated Proteins. *Curr. Protoc. Cell Biol.* **2007**, *35*, 24.2.1–24.2.11.
19. Freudiger, C. W.; Min, W.; Saar, B. G.; Lu, S.; Holtom, G. R.; He, C.; Tsai, J. C.; Kang, J. X.; Xie, X. S. Label-Free Biomedical Imaging with High Sensitivity by Stimulated Raman Scattering Microscopy. *Science* **2008**, *322*, 1857–1861.
20. Wang, M. C.; Min, W.; Freudiger, C. W.; Ruvkun, G.; Xie, X. S. RNAi Screening for Fat Regulatory Genes with SRS Microscopy. *Nat. Methods* **2011**, *8*, 135–138.
21. Dou, W.; Zhang, D.; Jung, Y.; Cheng, J. X.; Umulis, D. M. Label-Free Imaging of Lipid-Droplet Intracellular Motion in Early Drosophila Embryos Using Femtosecond-Stimulated Raman Loss Microscopy. *Biophys. J.* **2012**, *102*, 1666–1675.
22. Li, J.; Cheng, J. X. Direct Visualization of De Novo Lipogenesis in Single Living Cells. *Sci. Rep.* **2014**, *4*, 6807.
23. Wise, L. S.; Sul, H. S.; Rubin, C. S. Coordinate Regulation of the Biosynthesis of ATP-Citrate Lyase and Malic Enzyme During Adipocyte Differentiation. Studies on 3T3-L1 Cells. *J. Biol. Chem.* **1984**, *259*, 4827–4832.

DOI: 10.31635/ccschem.020.202000346
CCS Chem. **2020**, *2*, 1642–1648